Sensors & Actuators: B. Chemical 397 (2023) 134682

Contents lists available at ScienceDirect

Sensors and Actuators: B. Chemical

journal homepage: www.elsevier.com/locate/snb

NAP-XPS study of surface chemistry of CO and ethanol sensing with WO_3 nanowires-based gas sensor

Lesia Piliai [a], Thu Ngan Dinhová [a], Martin Janata [a], Dmytro Balakin [b,c], Stella Vallejos [d,e], Jaroslav Otta [b], Jitka Štefková [b], Ladislav Fišer [b], Přemysl Fitl [b], Michal Novotný [b], Jaromir Hubálek [d,f], Michael Vorochta [a,*], Iva Matolinová [a], Martin Vrňata [b,*]

[a] Department of Surface and Plasma Science, Faculty of Mathematics and Physics, Charles University, V Holešovičkách 2, 180 00 Prague 8, Czech Republic
[b] Department of Physics and Measurements, University of Chemistry and Technology Prague, Technická 5, 166 28 Prague 6, Czech Republic
[c] Institute of Physics of the NAS of Ukraine, Prospect Nauki, 46, Kyiv 03028, Ukraine
[d] CEITEC, Brno University of Technology, Purkyňova 123, 612 00 Brno, Czech Republic
[e] Instituto de Microelectrónica de Barcelona (IMB-CNM, CSIC), Campus UAB, Carrer dels Til·lers, Cerdanyola del Vallès, 08193 Barcelona, Spain
[f] Faculty of Electrical Engineering and Communication, Brno University of Technology, Technická 3058/10, 616 00 Brno, Czech Republic

ARTICLE INFO

Keywords:
WO_3 nanowires
Gas sensing mechanism
Operando study
Near-ambient pressure XPS

ABSTRACT

The nanowires prepared on a commercial Al_2O_3-based sensor platform were studied by near ambient pressure X-ray photoelectron spectroscopy (NAP-XPS) upon detecting CO and ethanol. Our findings indicated that the ex-situ prepared WO_3 NWs-based gas sensor might not be suitable for NAP-XPS studies, as the surfaces tend to accumulate significant carbon contamination, which remains on the surface even after long-term annealing in mbar range oxygen atmosphere at 593 K. To address this challenge, we developed a methodology involving exposure of the sensor to NO_x, which effectively cleans the surface and enables the detection of subtle chemical changes upon exposure to various carbon-containing analytes. Using NAP-XPS analysis, we investigated the gas sensing mechanisms of WO_3 NWs for CO and ethanol at different temperatures, revealing that it might combine several mechanisms commonly observed in metal-oxide chemiresistors. It is shown that the response to CO rather arises from the quick interaction of CO molecules with the ionosorbed oxygen. In the case of ethanol sensing, the main driving force for the sensor macroscopic electrical response at low temperatures is the adsorption of ethanol molecules. In contrast, at high temperatures, it combines the adsorption of ethoxy groups with the strong reducing effect of EtOH on the WO_3 surface.

1. Introduction

Tungsten trioxide (WO_3) is well known as a traditional material for sensitive layers in gas-detecting chemiresistors and has been reported/investigated for this purpose since 1967 [1]. The current research status of tungsten trioxide-based chemiresistors can be found in reviews such as [2–5]. When considering the use of tungsten trioxide or its "suboxides" in sensors, the following material properties should be taken into account: electrotransport properties, redox stability (tendency to form reduced phases of $WO_{3-\delta}$ stoichiometry with their characteristic surface- or volume-oxide vacancies), cation electronegativity related with Brönsted acidity, Lewis acidity, ferroelectricity, catalytic activity, crystalline structure and the existence of polymorphs, dominating orientation of surface facets, material dimensionality (bulk, 2D-, 1D- or 0D-nanostructures) and its relation to Debye length, specific surface of the material. Some of the above-mentioned characteristics are inherent to WO_3, the other ones are obtained secondarily as a consequence of the selected synthesis- and deposition method.

Tungsten trioxide is a typical n-type oxidic semiconductor (e.i. in an oxygen-containing atmosphere, the charge transfer is driven by an electron-depleted region on its surface) with bandgap $\Delta E_g = 2.7$ eV [6], which is somewhat less when compared to SnO_2 ($\Delta Eg = 3.6$ eV) - the most common oxide in gas sensing applications [7]. This implies that WO_3 should have a less pronounced temperature dependence of specific resistivity. However, the authors in Ref. [8] have observed that a mixed phase containing sub-stoichiometric monoclinic $WO_{2.83}$, $WO_{2.92}$, and tetragonal W_5O_{14} exhibited p-type response behavior to ethanol (EtOH) and methanol vapors at room temperature (RT) and also a p-type

* Corresponding authors.
E-mail addresses: vorokhtm@mbox.troja.mff.cuni.cz (M. Vorochta), martin.vrnata@vscht.cz (M. Vrňata).

https://doi.org/10.1016/j.snb.2023.134682
Received 21 July 2023; Received in revised form 24 September 2023; Accepted 24 September 2023
Available online 26 September 2023

response to NO_2 at slightly elevated temperatures in the range 25–50 °C that converted to n-type response at 50–250 °C. Similarly, in Ref. [9], the sensor based on the $W_{18}O_{49}$ phase has a p-type response when detecting ammonia. In general, as tungsten trioxide tends to form surface or volume oxygen vacancies associated with this sub-stoichiometry (often marked as $WO_{3-\delta}$), it is always very important to check the concentration of oxidic vacancies in the material. On the other hand, there are indications that WO_3 or $WO_{3-\delta}$ are not reduced to WO_2 during sensing performance, as no works report the formation of the WO_2 phase in sensitive layers. Furthermore, it seems that the role of surface- and volume-oxygen vacancies in the detection process is rather different; while the volume affects mainly the material conductivity, the surface provides particularly reactive sites for gas adsorption and molecular reactions [10].

The electronegativity of tungsten achieves $\chi_W = 2.36$, which is the second-highest value of all metals (just after gold). This circumstance, together with the high tungsten oxidation state (6+), makes WO_3 to be probably the most acidic (Brönsted acidity) of all usual gas-sensitive oxides, including SnO_2, In_2O_3, TiO_2, ZnO, CuO or ZrO_2, which can explain the good sensitivity of WO_3 oxide to basic gases (ammonia, hydrazine) [11]. In addition, due to its electronic structure, WO_3 can accept lone pair of electrons into its empty orbital, thus acting as a Lewis acid [12], which allows the detection of all gases that exhibit Lewis basicity, e.g. CO, HCN, cyanogen. It is supposed that these Lewis acid - Lewis base reactions can occur even at RT [13], which allows the design of chemiresistors with low power consumption. Another effect that may favor the interaction of WO_3 or $WO_{3-\delta}$ with polar gases - is the existence of material ferroelectricity, especially when the crystal symmetry is lower and oxygen vacancies are present. Under such circumstances, a spontaneous electric dipole moment in the material is formed, and it can spontaneously interact with the molecular dipole moment of gaseous analytes. Thus, the monoclinic WO_3 phase exhibited significantly higher sensitivity to acetone vapors than the hexagonal phase [14]. This phenomenon is attributed to the different polarity coming from the crystal geometry. Monoclinic WO_3 with oxygen vacancies is ferroelectric due to the displacement of the charge center of $[WO_6]$ octahedra. Tungsten oxide also has pronounced catalytic behavior in the total oxidation of volatile organic compounds. In Ref. [15], the authors observe the oxidation of benzene, toluene, and xylene into CO_2 and H_2O in a wide range of operating temperatures (50–450 °C). The high catalytic activity stems from the high concentration of surface-oxygen vacancies, which stimulates the chemisorption of reactive oxygen species from the atmosphere. In any case, not only aromates but also other gaseous analytes can be easily oxidized on the tungsten oxide surface, so in reality, the products of their oxidation are detected.

Tungsten trioxide is known to have at least five polymorphs - monoclinic, triclinic, orthorhombic, hexagonal, and cubic. Its crystals are generally formed by corner or edge-sharing of $[WO_6]$ octahedra. A comprehensive crystallographic review of tungsten trioxide is given in Ref. [16]. WO_3 is characterized by nonstoichiometric properties, as the lattice can withstand a considerable amount of oxygen deficiency, expressed formally as $WO_{3-\delta}$, where the value of δ strongly affects the electronic band structure and resistivity of the material. For $\delta \geq 0.13$ (e.g. in $W_{18}O_{49}$), the pure-octahedra structure becomes unstable and partial restructuring occurs. All these polymorphs differ in ability to interact with gases (e.g. hexagonal WO_3 contains typical hexagonal and trigonal tunnels inside its structure, which can be advantageous for gas sensing) [12]. Another aspect of this topic - the gas sensing response of semiconductors is a surface-controlled process. Hence it also depends on the crystal orientation of the individual oxide grains in the sensitive layer, and therefore the use of so-called "faceted engineering" (i.e. stimulating preferential growth of certain crystal orientation during the deposition of the sensitive layer) can be a helpful tool for improving the sensing process. It has been shown that the (010) facets of triclinic WO_3 had a better response to 1-butylamine, while the (002) ones exhibited a stronger response to acetone [17]. A more detailed view revealed that in the monoclinic phase, the surface energy of facets (and also sorption capacity for oxygen species) decreases in the sequence (002) > (020) > (002). Consequently, the response to reducing gases will also decrease in this sequence. At the same time, the reaction to oxidizing analytes (such as NO_2) will be strongest for (002), as in this latter case, there is the weakest competition between O_2 and NO_2 species [18].

As for other oxidic materials, three generalized sensing mechanisms are often reported for WO_3 [19]: a) "Ionosorption model", where ionosorption of negatively charged oxygen species plays a crucial role leading to the formation of depleted regions in the oxide. Subsequent reaction of these oxygen species with the target analyte is accompanied by electron exchange and modulation of intergrain resistance. b) "Oxygen-vacancy model" - this mechanism accents reversible partial reduction and reoxidation of the oxidic surface. The partial reduction of the oxide by e.g. ethanol can cause the formation of additional oxygen vacancies associated with the injection of electrons into the conduction band. As soon as the analyte is oxidized, the oxide surface interacts more intensively with atmospheric oxygen, the vacancies are filled, and the sensitive layer restores its original resistance. c) "Direct adsorption model" - according to this description, the molecules of an analyte can absorb directly onto the oxidic surface without any reaction with ionosorbed oxygen [10]. Of these three mechanisms, the c) is less commonly discussed/accepted, but e.g. in Ref. [20] spectroscopic studies confirm that the molecule of detected acetone absorbs via the oxygen of its carbonyl into the oxygen vacancy of the $WO_{3-\delta}$ surface. For ethanol, it has been proposed that its adsorption occurs in the form of ethoxy species, followed by the subsequent desorption of hydrogen and acetaldehyde, but certainly, these products can be subjected to consecutive reactions. A similar mechanism, which included the formation of acetaldehyde during the detection of ethanol, was also observed for ZnO-based chemiresistors [21].

Each detection process is based on direct interaction between the sensitive layer and an analyte molecule. This trivial fact implies that not only the material properties of tungsten trioxide discussed above but also the characteristics of the analyte molecule will co-determine the detection parameters. The following "molecular descriptors" should be taken into account: redox properties, presence and spatial orientation of the dipole moment, Brönsted acidity, and Lewis acidity. The contribution of redox properties has been discussed many times - regardless of the detailed mechanism (which can be rather complicated), the reducing gases act as electron donors and the oxidizing ones as electron acceptors, thus modulating the resistance of the sensitive semiconductive layer accordingly. As for the molecular dipole moment - when present, it interacts with the spontaneous dipole moment of ferroelectric $WO_{3-\delta}$. For example, in Ref. [19], the authors state that the dipole moment of the acetone molecule qualifies the adsorption geometry with the carbonyl group pointing towards the oxidic surface, which is discussed in detail also in Ref. [14]. We have already mentioned that tungsten trioxide behaves like both Brönsted acid and Lewis acid. Based on this premise, one should suppose that WO_3 will easily detect gaseous molecules with complementary properties - i.e. either Brönsted or Lewis bases (ammonia, organic amines, hydrazine, alcohols, aldehydes, carbon monoxide, cyanogen, etc.). However, this simple scheme may be complicated by water molecules, which are always present in the environment and can be easily protonated/deprotonated and also act as a strong Lewis basis. The resistance of WO_3 was found to increase in the presence of atmospheric humidity - this is the opposite behavior compared to SnO_2-based sensors. Also, when detecting carbon monoxide, the WO_3 sensors respond better in humid air than in dry conditions, unlike the SnO_2 ones [20].

The current debate on the detection mechanism of different analytes by WO_3-based chemiresistors suggests the need for further investigation. In recent years, in-situ/operando techniques have been used to study gas sensors and shed light on this problem [22,23]. The advantage of such an approach is to obtain information about the surface chemistry of a gas sensor operating under conditions closer to those occurring during the

real detection process. The most commonly used analytical techniques in operando studies of gas sensors are diffuse reflectance infrared Fourier transform spectroscopy (DRIFTS) [24,25], UV visible spectroscopy (operando UV-Vis) [26], Raman spectroscopy [27,28], X-ray absorption (XAS) and emission (XES) spectroscopies [29]. However, it should be mentioned that one of the most powerful techniques for surface-sensitive chemical analysis of a solid surface in the presence of gas is near-ambient photoelectron spectroscopy (NAP-XPS) [30,31]. We have recently successfully utilized NAP-XPS to study the EtOH and NO_x detection mechanisms of several different chemiresistive materials [21, 32–34]. It was demonstrated that NAP-XPS could provide information about the presence of various surface-intermediated species and the formation of surface vacancies while detecting reducing gases or their disappearance upon exposure to the oxidizing analytes. In this work, we applied the NAP-XPS technique to investigate the interaction of WO_3 nanowires (NWs)-based gas sensors with NO_x, CO, and EtOH to contribute to understanding their detection mechanisms.

2. Experimental section

2.1. Synthesis of WO_3 nanowires and fabrication of WO_3-based gas sensor

WO_3 NWs were synthesized by aerosol-assisted chemical vapor deposition (AACVD) directly on the top of a commercial Al_2O_3-based sensor platform with platinum interdigitated electrode structures (IDES) separated by 15 μm gap (KBI2 Tesla Blatná a. s.). The synthesis process was performed at 390 ºC using a solution of tungsten hexacarbonyl (20 mg, $W(CO)_6$, Sigma-Aldrich, ≥ 97%) and methanol (5 ml, Sigma-Aldrich, ≥99.6%) as previously reported [35]. The aerosol droplets from the solution were generated using a piezoelectric ultrasonic atomizer (Liquifog, Johnson Matthey) operating at 1.6 MHz and transported to the heated sensor platform by a nitrogen gas flow (200 cm^3 min^{-1}). The time taken to transport the entire volume of solution was typically 45 min. These conditions allowed for the formation of a light blue color uniform film over the Al_2O_3-based sensor platform. The prepared sensor was then annealed at 500 ºC for two hours in the air, changing the WO_3 NWs color from light blue to white. It was essential to have a high density of NWs completely covering the IDES area and ensuring the elimination of its signal during the NAP-XPS measurements, as it could contribute to the O 1s and C 1s spectra from the WO_3 NWs layer, thus distorting them.

2.2. Morphological and structural characterizations

The distribution, morphology, and crystal structure of WO_3 NWs were observed by a scanning electron microscope (SEM) *Tescan MIRA 3* and a transmission electron microscope (TEM) *JEOL 2200FS* operated at electron beam energy 30 keV and 200 keV, respectively. The distribution of WO_3 NWs deposited on the sensor platform was studied via low-magnification SEM images. The morphology and crystal structure were characterized by TEM using high-resolution TEM (HRTEM) and selected area electron diffraction (SAED) technique. For TEM measurement, WO_3 NWs were wiped onto a holey carbon-coated copper 300-mesh grid (Agar Scientific), and *Digital Micro-graph* software was used for TEM image analysis.

2.3. In-situ near-ambient pressure X-ray photoelectron spectroscopy characterization and measurement of chemiresistor properties at low pressure

A laboratory NAP-XPS system (SPECS Surface Nano Analysis GmbH) was utilized to conduct the NAP-XPS measurements. The system was equipped with a monochromatized Al Kα X-ray source, a hemispherical electron energy analyzer, and a specially designed NAP cell [32]. The WO_3 NWs-based gas sensor was mounted on a sample holder that, along with the NAP-XPS measurements, also allowed in-situ observation of the sensor resistance by applying a constant voltage of 0.1 V to its contacts. Based on these measurements, the so-called low-pressure (LP) chemiresistor properties were evaluated. During the NAP-XPS measurements, W 3d, O 1s, and C 1s XPS spectra were recorded at a constant pass energy of 20 eV and a photoelectron emission angle of 0° with respect to the sample normal. The following steps were taken to investigate the interaction of the sensor with low concentrations of EtOH and CO. The spectra were first acquired at 593 K in 1 mbar of oxygen, thus mimicking the ambient atmosphere without a reducing agent, and then in 1.2 mbar of O_2/EtOH and O_2/CO mixtures prepared by adding 0.2 mbar of EtOH vapor or CO gas to the oxygen. The study was also collected at 593 K in 0.2 mbar of EtOH or CO only. Between each dosing, the surface was refreshed by exposing it to 1 mbar of O_2 for 30–90 min. The interaction of the sensor with NO_x was studied by exposing it to 1 mbar of O_2 containing 1% of NO_x. After the NO_x exposure, the experiment with CO and EtOH was repeated at 593 and 373 K. Ar+ sputtering, which is used to create oxygen vacancies on the sensor surface, was performed at room temperature using 1000 eV Ar ions incident on the surface at an angle of 45 degrees. The NAP-XPS core-level spectra were fitted with a Voigt profile after subtracting the Shirley background using the KolXPD fitting software.

2.4. Measurement of chemiresistor properties of WO_3 NWs at atmospheric pressure

Apart from investigating sensor resistance in-situ during NAP-XPS characterization, which resulted in the evaluation of LP chemiresistor properties, it was also necessary to explore the chemiresistor properties of WO_3 NWs- based sensors in real conditions, i.e. under atmospheric pressure (abbreviated as AP chemiresistor properties). The concentration of EtOH, CO, or NO_2 was 10 ppm in synthetic air, reference gas "pure" synthetic air (Linde Gas a.s.) containing < 0.05 ppm of hydrocarbons. These AP chemiresistor measurements were carried out on the same sensor substrates as described in Section 2.1. The measuring apparatus is depicted in Fig. S1 of the Supporting Information (SI). It is constructed as a continuous-flow system containing Tedlar sample bags, a sampling valve, a chamber with a sensor, pump, valve for gas-flow setting and rotameter. The VITON connecting tubes have a diameter of 3 mm; the SWAGELOG sampling valve and chamber-feedthroughs are used. The measuring chamber has an internal volume of 110 ml (material - PEEK, equipped with stainless steel insert, which serves as electromagnetic shielding). The gas flow rate was kept at 80 ml min^{-1}.

3. Results and discussion

3.1. Structural analysis and AP chemiresistor properties of the WO_3 nanowires

The SEM image of the WO_3 NWs deposited on the sensor platform is shown in Fig. 1a. It can be seen that the NWs with a length of about 10 μm formed a well-distributed carpet-like layer that completely covered the surface of the platform. TEM examination of a single WO_3 NW (Fig. 1b-d) revealed that the individual NWs were 100–150 nm thick and entirely crystalline. HRTEM and SAED patterns verified the monoclinic phase of the tungsten oxide with a lattice spacing of 0.40 nm, corresponding to the (002) lattice plane. These results are in good agreement with the previous XRD analysis of the WO_3 NWs, which evidenced diffraction patterns associated with the monoclinic phase of WO_3 (ICCD card no.72–0677) [35].

The AP chemo-resistive properties of the fabricated WO_3 NWs-based sensor were investigated by measuring its responses to 10 ppm of NO_2, CO, and EtOH at T_{oper} = 593 K. Its measured resistance in air at room temperature was about 10 kOhm. After reaching the operating temperature, the baseline resistance of the sensor measured in the air dropped to about 450–600 Ω. It showed excellent reactions to NO_2 and

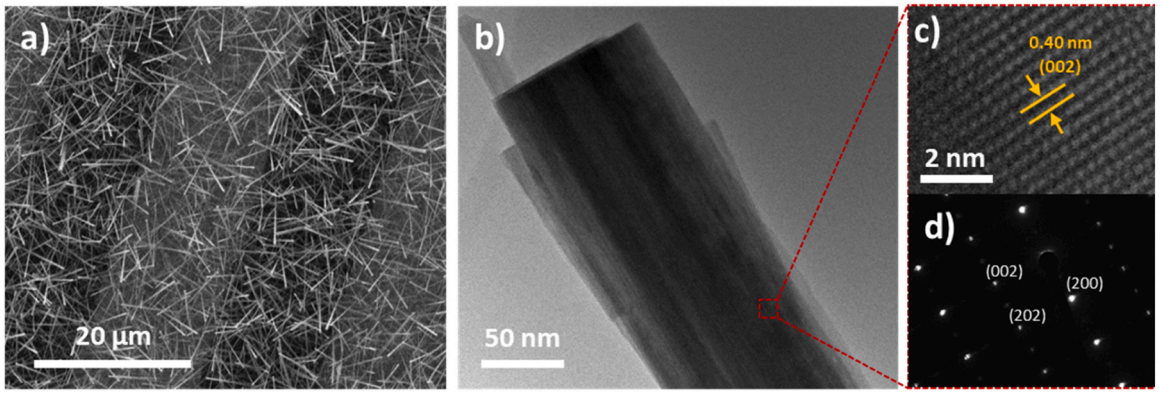

Fig. 1. (a) WO_3 NWs deposited on the sensor platform, (b) low-magnification TEM image of a single WO_3 NWs, (c) and (d) high-resolution HRTEM image of the NW and its corresponding diffractogram, respectively.

slightly smaller but satisfying responses to CO and EtOH (Fig. S2 of SI).

3.2. In-situ NAP-XPS study

The WO_3-based gas sensor was loaded into the evacuated high-pressure cell of the NAP-XPS spectrometer, exposed to 1 mbar of O_2 at room temperature, and subsequently heated to 593 K. The acquisition of the W 4f XPS spectrum in UHV at room temperature (top spectrum in Fig. 2a) showed that the NWs mainly consist of WO_3, giving rise to the doublet with the main peak binding energy (BE) at about 35.7 eV [36, 37]. The presence of a small state at about 34.6 eV assigned to WO_x ($x < 3$) indicated that the surface of the NWs is slightly reduced, probably due to various surface defects and inhomogeneities [37]. The presence of the defects could also be seen from the asymmetry of the corresponding O 1s spectrum in Fig. 2b, typically indicating the presence of hydroxylated oxygen vacancies on the surface of oxides [38] or different oxygen-containing hydrocarbon impurities [39]. The corresponding C 1s (Fig. 2c) showed that the as-received WO_3 NWs contain a relatively high amount of adventitious carbon on their surface. Heating of the WO_3 NWs in the O_2 atmosphere resulted in complete surface reoxidation, leading to the disappearance of the WO_x state in the W 4f spectrum (bottom spectrum in Fig. 2a) and also to a slight decrease of the signal at 532 eV in the corresponding O 1 s spectrum. It should be mentioned that the heating in O_2 also shifted all spectra to lower BE by about 0.2 eV compared to their positions at room temperature. We believe this is due to the band-bending effects caused by the oxygen ionosorption on metal oxides [32]. However, in order to detect changes in the shape of C 1s, O 1s, and W 4f spectra, we eliminated this shift in Fig. 2 for all spectra measured in O_2. The corresponding C 1s spectrum revealed only a very moderate reduction in the amount of surface carbon on heating in the O_2 environment.

The electrical resistance of the sensor, monitored simultaneously with the NAP-XPS measurements, showed that the loading of the sensor to the NAP cell and subsequent evacuation results in its room temperature resistance of about 2 kOhm (Fig S3 of SI). The exposure to 1 mbar of O_2 and heating to 593 K caused a decrease of the sensor's resistance to about 200 Ohm. The low initial sensor resistance R_0, arising from the high density of WO_3 NWs required for the NAP-XPS measurements, resulted later in generally lower responses of the sensor to the analytes but, at the same time, showed a very low noise level.

The in-situ responses of the WO_3 NWs-based sensor on the addition of EtOH and CO to the oxygen and upon exposing it to 1 mbar of 1% NO_x/O_2 mixture are presented in Fig. 3. The sensor exposing to the O_2/EtOH mixture initiated a well-seen and quick in-situ LP response corresponding to n-type semiconductor (Fig. 3a). However, the recovery of the sensor after stopping the EtOH dosing and exposing it again to 1 mbar O_2 was significantly prolonged. The baseline continued to recover even during the following CO exposure, causing however a much

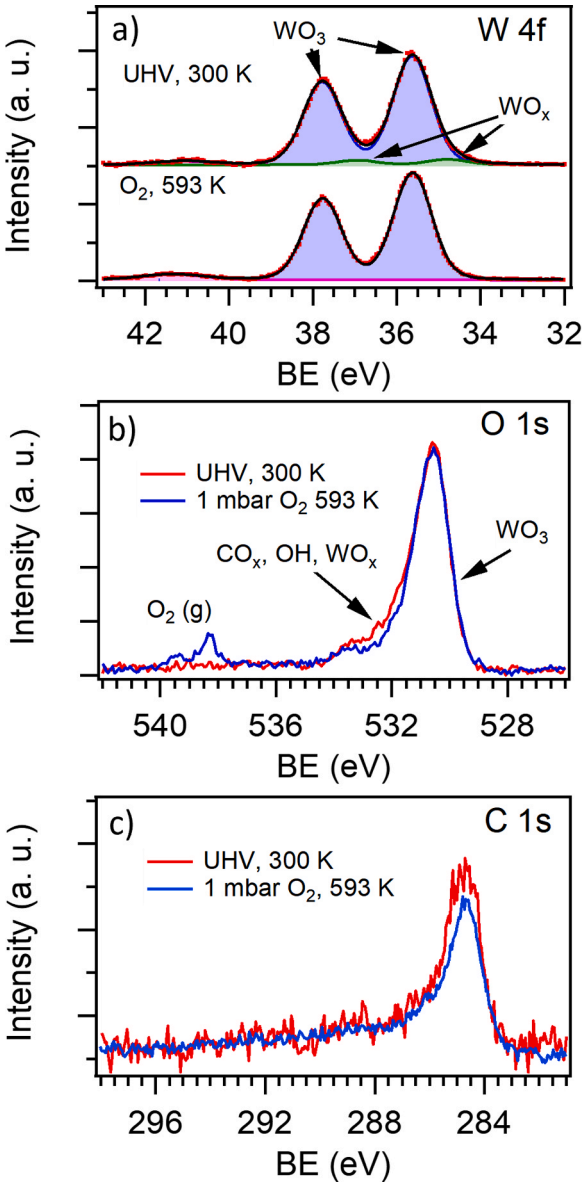

Fig. 2. NAP-XPS W 4f (a), C 1s (b), and O 1s (c) spectra collected from the as-prepared WO_3 NWs in UHV at RT and in the presence of 1 mbar O_2 at 593 K.

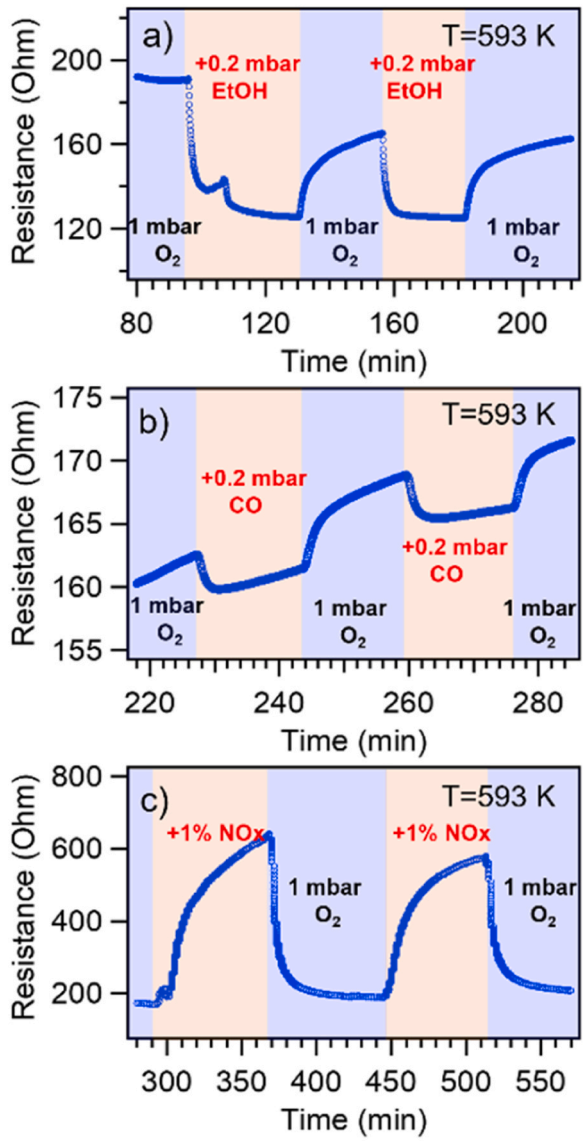

Fig. 3. Responses of the as-prepared WO_3 NWs-based chemiresistor to ethanol (a), CO (b), and nitrogen dioxide (c) at T_{oper} = 593 K inside the high-pressure (NAP) cell of the NAP-XPS spectrometer.

smaller response than in the case of ethanol (Fig. 3b). Finally, exposing the sensor to the O_2/NO_x mixture demonstrated a fast positive response of much higher amplitude and quick recovery to the initial state after switching the atmosphere back to O_2 (Fig. 3c).

The LP responses were generally analogous to the AP measurements presented in Fig. S2 of SI. For the CO and EtOH sensing, the LP baseline value (approx. 200 Ω) was slightly lower than the AP one (approx. 500 Ω). However, this is not an order-of-magnitude difference and can be attributed to the significantly lower partial pressure of oxygen in the standard atmosphere. There was an apparent similarity between the AP and LP responses of the chemiresistor to EtOH. In both cases, the first response was higher than the following ones, and the initial value of the sensor baseline did not recover in the subsequent measurement cycles. For CO, the LP responses were significantly lower than the AP responses and were accompanied by the baseline drift, indicating the importance of oxygen in the detection mechanism. In the case of NO_x detection, the AP and LP responses to NO_2 are almost identical.

The NAP-XPS spectra obtained when the sensor was exposed to the O_2/EtOH and O_2/CO mixtures and pure EtOH and CO gases at 593 K are presented in Fig. S4 of SI. By comparing them with the spectra measured in O_2, a slight shift of about 0.1–0.2 eV to higher BE with respect to the peak positions in O_2 can be noticed. A similar shift has already been observed in the case of exposing other oxides to an EtOH-containing atmosphere [32]. It is probably related to the change in the surface work function caused by the mixed effect of decreased chemisorbed oxygen concentration and analyte adsorption on oxide surfaces. Apart from these shifts, a surface reduction was seen from the W 4f spectrum measured in EtOH and tiny changes in the corresponding C 1s and O 1s regions. Because of the substantial surface carbon contamination, assigning them to the presence of any species resulting from CO or EtOH exposures was impossible. The NAP-XPS measurements performed during the O_2/NO_x exposure showed that NO_x also substantially affects the sensor surface. First, it affected the position of all the NAP-XPS peaks, shifting them by a further 0.3 eV to lower BE. This shift, resulting from the adsorption of NO_x species on the sensor surface, was well seen by comparing the as-measured W 4f spectra acquired in O_2 and O_2/NO_x, respectively, as shown in Fig. S5 of SI. We tried to detect the adsorbed NO_x species by measuring the N 1s spectrum of the sensor exposed to the O_2/NO_x mixture, but unsuccessfully. It seems that the coverage of the adsorbed NO_x species is below the XPS detection limit. Eliminating the NO_x-induced shift from the spectra measured in O_2/NO_x and comparing them with the spectra obtained in O_2 demonstrated that the NO_x exposure also had a cleaning effect on the sensor surface. It was completely free from all carbon contamination after approximately 90 min of O_2/NO_x exposure (Fig. 4a, b). At the same time, the comparison of the W 4f spectra (Fig. 4c) showed no changes in the spectrum shape during the NO_x exposure.

As the O_2/NO_x exposure substantially influenced the sensor surface, we decided to repeat the CO and EtOH exposures and see how the NO_x treatment affected the functionality of the sensor. In the case of prevailing ionosorption or direct adsorption models in the sensing mechanism of EtOH and CO by the WO_3-based sensor, the opening of additional adsorption sites was expected to increase the sensor's response. The in-situ measured LP responses to CO of the cleaned WO_3 NWs-based sensor presented in Fig. 5a showed that, despite the surface cleaning, the sensor responses remained almost the same as in the case of the "contaminated" sensor. In the case of EtOH detection (Fig. 5b), the reaction of the sensor on the first EtOH dosing was a bit higher than before the NO_x exposure; however, the recovery was worse. The sensor recovered to only approximately 50% of its initial resistance after about 20 min of the O_2 exposure. The second EtOH pulse returned the sensor resistance to the same response level as during the first exposure, indicating a saturation EtOH layer formed on the surface during each exposure that is not dependent on the amount of the preadsorbed species.

The NAP-XPS spectra obtained while exposing the cleaned sensor to O_2/CO are presented in Fig. 6. In the case of CO, the NAP-XPS measurements showed practically no CO adsorption on WO_3 NWs, neither in the presence of CO/O_2 nor even CO. The only peaks detected upon both exposures in the corresponding C 1 s spectra (Fig. 6a) were the small peaks at about 284.6 eV and gas phase peaks at about 291 eV. The position of the first peak corresponds rather to -CH_x and C-C bonds, and it probably arose from some carbon contamination that accumulated on WO_3 NWs during the longtime CO exposures. The states of C-O and C═O species, typically located at 286 and 289 eV, respectively, were absent. Finally, CO molecules demonstrated a slight ability to reduce the surface of WO_3 NWs, as can be seen from the corresponding O 1s and W 4f spectra collected in CO (Fig. 6b and c). Thus, it can be concluded that the CO detection mechanism of the WO_3 NWs-based sensor most probably involves the interaction of CO molecules with the chemisorbed or bulk oxygen atoms rather than its direct adsorption on the surface.

The NAP-XPS spectra obtained while subsequently exposing the cleaned sensor to O_2, O_2/EtOH, EtOH, and O_2 again are presented in Fig. 7. The C 1s spectrum measured in the presence of O_2/EtOH (the second spectrum from the bottom in Fig. 7a) demonstrated the presence of intermediate surface species on WO_3 NWs during the exposure. The

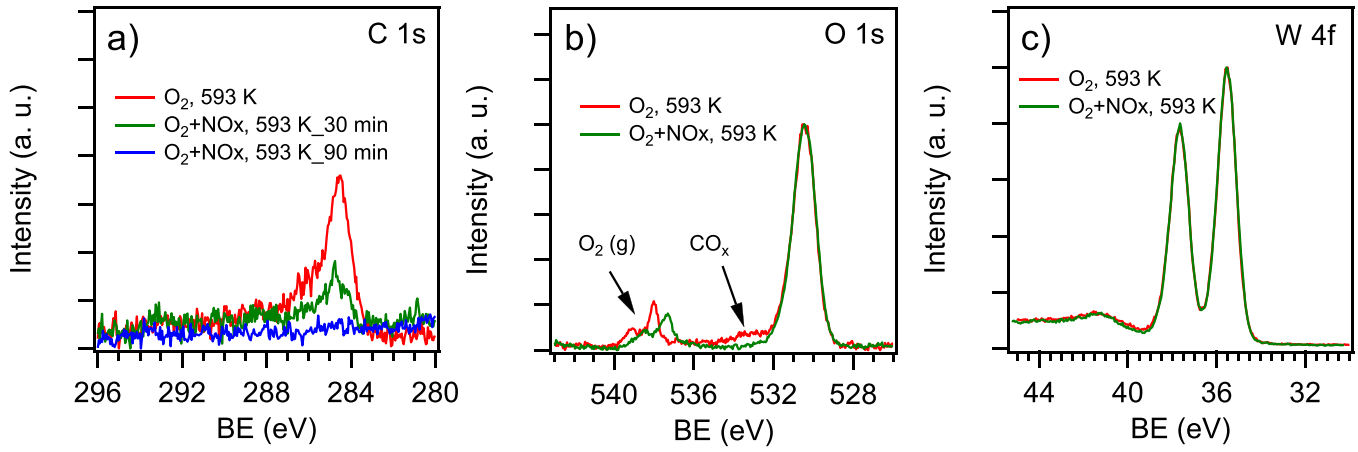

Fig. 4. C 1s (a), O 1s (b), and W 4f (c) NAP-XPS spectra acquired from the WO_3 NWs in the presence of 1 mbar O_2 and 1%NO_x/O_2 gas mixture at 593 K. The spectra measured in the O_2/NO_x mixture are shifted by 0.3 eV to higher BE to eliminate the band-bending effects caused by NO_x adsorption.

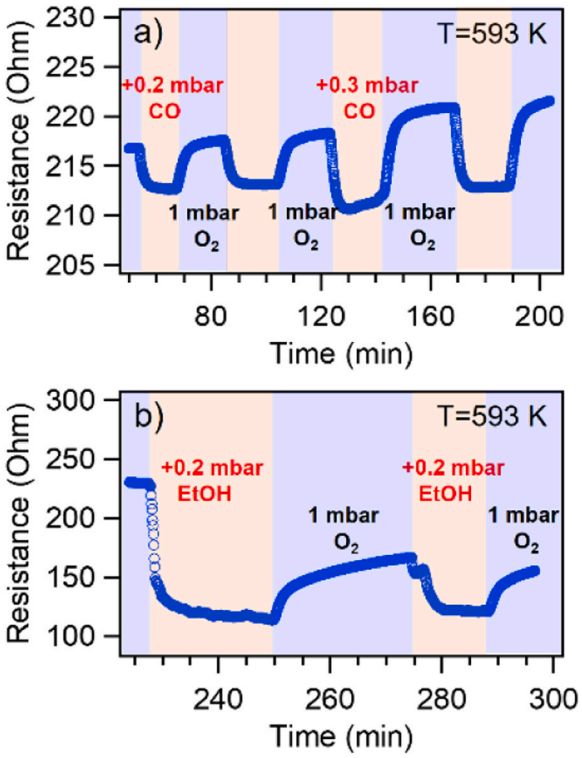

Fig. 5. LP responses of the cleaned WO_3 NWs-based chemiresistor CO (a) and EtOH (b) at T_{oper} = 593 K.

fitting of this spectrum shows that the surface might be covered by ethoxy species typically indicated by the two peaks separated by about 1.3 eV corresponding to the methyl (CH_3-) and alkoxy (-CH_2O-) carbons [40]. The presence of entire ethanol molecules adsorbed on the surface cannot be ruled out either. Their XPS signal should also contain two peaks of the methyl and hydroxymethyl (-CH_2-OH) groups. These two peaks of neutral ethanol molecules separated by about 1.5 eV can be seen from the C 1s spectrum of the ethanol gas phase (the top spectrum in Fig. 7a). The carbon signal in the presence of only EtOH (the third spectrum from the bottom in Fig. 7a) was practically the same as in the O_2/EtOH mixture concerning the intensity and shape. At the same time, the corresponding O 1s and W 4f spectra presented in Fig. 7b and c indicated a partial reduction of the surface. It evidences that EtOH molecules should be partially oxidized to ethoxy groups, releasing hydrogen atoms that reduce the sensor surface. However, the absence of carbonyl, carbonate, formyl, and carboxylate groups in the C 1s spectrum (typically present at BE of 288–290 eV) clearly shows ethanol decomposition on WO_3 NWs at 593 K no further than to ethoxy species (either in the presence or absence of O_2).

After studying the surface chemistry of the sensor at 593 K, we decided to decrease its working temperature to 393 K and investigate it again. According to the ionosorption model, the charged oxygen ions (O^-_{ads}), which are the most reactive and sensitive to the reducing agent, are expected to appear on the surface of metal oxides exposed to oxygen only at temperatures above 423 K [41]. At lower temperatures, O_2 molecules should adsorb nondissosiatively as the superoxide O_2^- ions, which are considered less important in gas sensing [42]. Also, at this temperature, the reduction of the WO_3 surface by CO or EtOH is very unlikely. Therefore, if the ionosorption or oxygen-vacancy mechanisms prevail in the detection of CO and EtOH by the WO_3 NWs-based chemiresistor, it should show little or no sensor response. The results presented in Fig. 8a indeed showed an almost indetectable reaction of the sensor to CO at 393 K. In the case of EtOH detection (Fig. 8b), the response was better detectable but with a much lower amplitude than at 593 K. The EtOH exposure also caused the drifting of the sensor baseline. During the subsequent O_2 exposures, the sensor resistance was recovered only by the value of its drop in the first several minutes of EtOH exposure, while the decrease due to the prolonged EtOH exposure remained unrecovered. It indicated that different reversibly and irreversibly adsorbing species might occur during the EtOH exposure of WO_3 NWs at 373 K, causing reversible and irreversible changes in the sensor resistance. Measuring the C 1s spectra during the O_2/CO and O_2/EtOH exposures at 373 K (Fig. 8c) revealed similar results to those obtained at 593 K. Initially, during the O_2 exposure, there was present only a tiny amount of some carbon contamination accumulated on the surface. Adding CO to the atmosphere did not change the appearance of the C 1s spectrum, indicating no CO adsorption on the WO_3 NWs even at low temperatures. Regarding O_2/EtOH exposure at 393 K, the corresponding C 1s spectrum showed a similar adsorbed EtOH-derived species on the surface as at 593 K. However, the sensor at the low temperature showed a much lower rate of their desorption in the O_2 atmosphere. The accumulation of a high amount of carbon contaminations was observed, which was most likely responsible for the continuous drift of the sensor baseline.

After analyzing the obtained results, it is clear that only one model cannot wholly describe the CO and EtOH sensing mechanisms of the WO_3 NWs-based chemiresistor. It is probably a combination of several sensing models generally reported for the metal-oxide chemiresistors. In the case of CO, it appears that CO molecules adsorb on the surface of WO_3 NWs, neither at 593 K nor at 393 K, and cannot act as direct

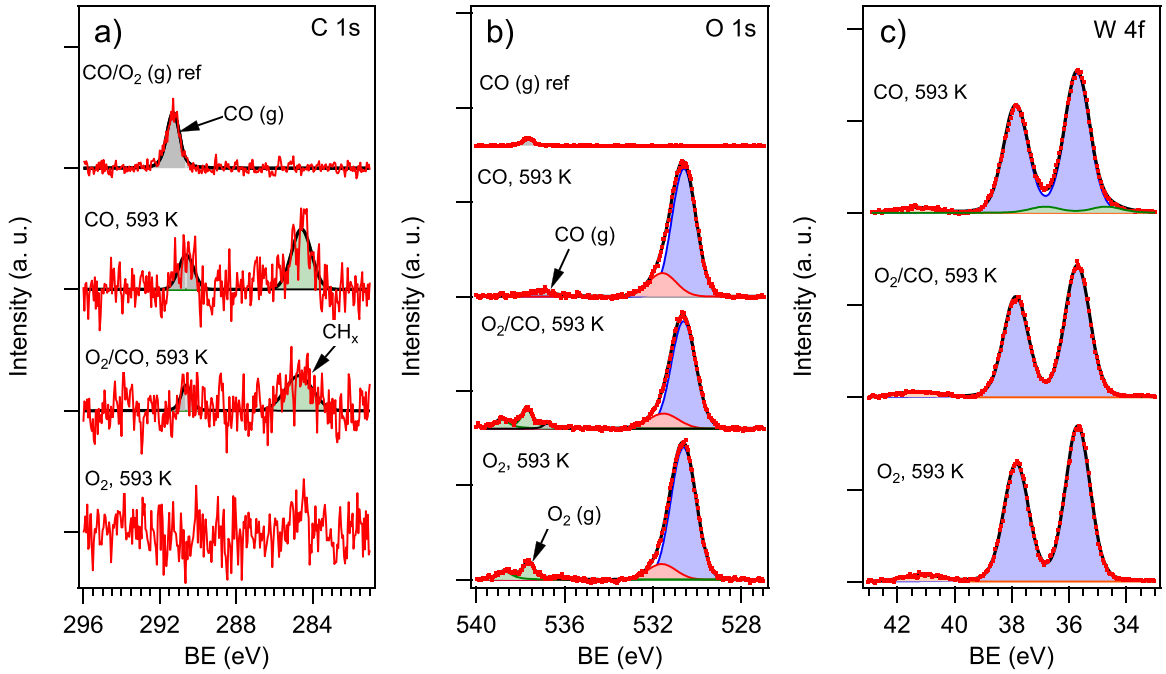

Fig. 6. C 1s (a), O 1s (b), and W 4f (c) NAP-XPS spectra acquired from the cleaned WO_3 NWs-based sensor while exposing it to O_2, O_2/CO, and CO. The topmost spectra in the C 1s and O1s regions are the reference spectra of CO gas.

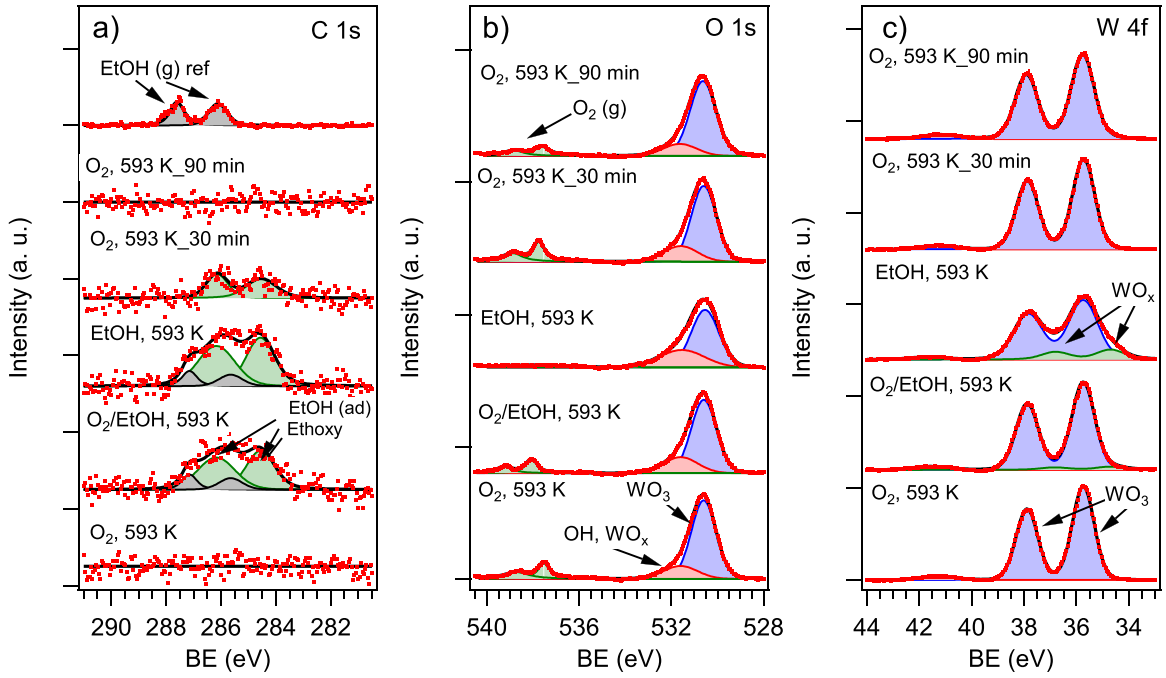

Fig. 7. C 1s (a), O 1s (b), and W 4f (c) NAP-XPS spectra acquired from the cleaned WO_3 NWs-based sensor while exposing it to O_2, O_2/EtOH, EtOH, and again O_2. The topmost spectrum in the C 1s region is the reference spectra of EtOH vapor.

electron donors for the surface. However, they interact with the WO_3 surface at high temperatures, probably decreasing the ionosorped oxygen concentration and creating some not detectable by XPS low amount of surface oxygen vacancies. This explains the detectable chemiresistor response at 593 K and why there is almost no reaction to CO at 393 K, the temperature at which no chemisorbed atomic oxygen is present on the surface, and when CO cannot reduce the bulk oxide.

On the contrary, exposing the WO_3 NWs-based sensor to the EtOH-containing atmospheres showed that there is always a certain amount of adsorbed EtOH-related species on the surface. The comparative NAP-XPS analysis performed at different temperatures and presented in Fig. 9 showed that the amount and type of those species are temperature dependent. As seen from Fig. 9a, demonstrating the absolute C 1s signal of the adsorbed species on the surface of WO_3 NWs exposed to O_2 at 593 K and the O_2/EtOH mixture at 593, 493, and 393 K, the amount of the adsorbed EtOH molecules increases with decreasing surface temperature. In addition, the peak positions of the methyl (CH_3-) and alkoxy (-CH_2O-) carbons in the ethoxy groups, which are present on the surface

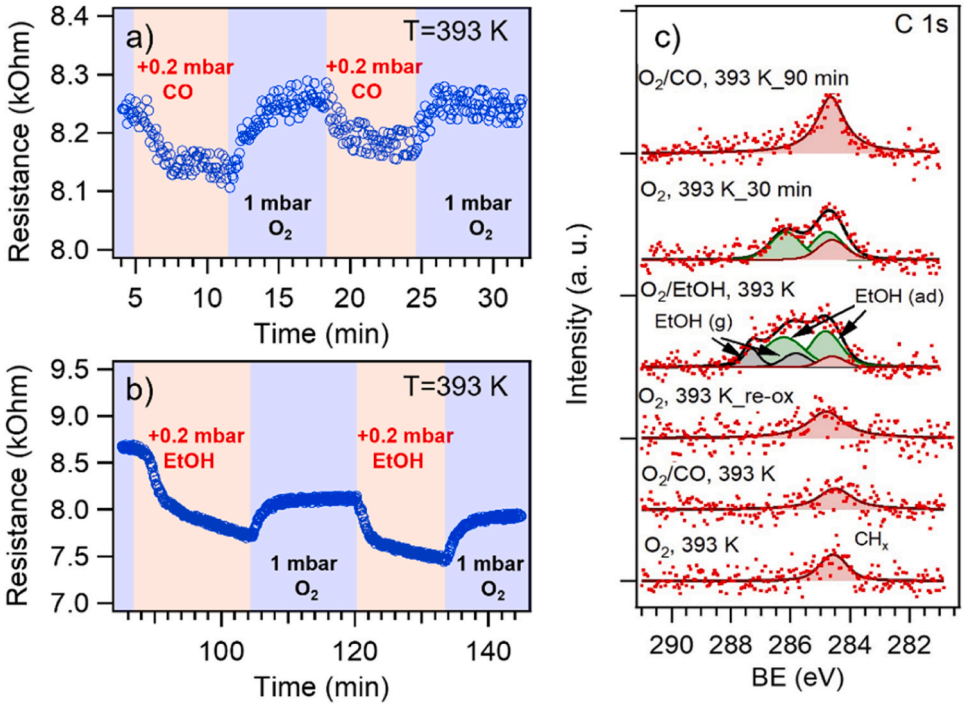

Fig. 8. LP responses of the WO_3 NWs-based chemiresistor to CO (a) and EtOH (b) at T_{oper} = 393 K. (c) C 1s NAP-XPS spectra acquired from the WO_3 NWs-based sensor while exposing it to different analytes at 393 K.

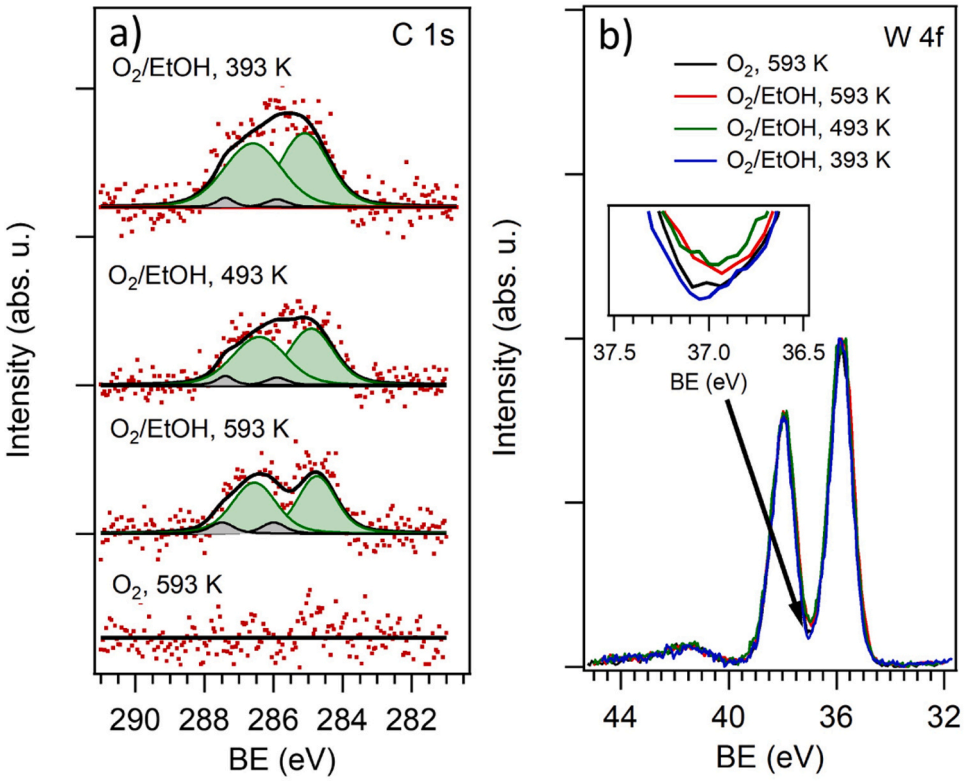

Fig. 9. C 1s (a) and W 4f (b) NAP-XPS spectra acquired from the clean WO_3 NWs-based sensor while exposing it to 1 mbar of O_2 at 593 K and upon subsequent O_2/EtOH exposures (1.2 mbar) at different temperatures.

at 593 K, shift to a higher BE with decreasing temperature. It indicates that some adsorbing EtOH molecules probably do not oxidize to ethoxy but adsorb in the molecular form at lower temperatures. The corresponding W 4f spectra depicted in Fig. 9b also support this suggestion. Indeed, from the inset image, showing the part of W 4f doublet of WO_3 at about 37 eV, it can be seen that exposing the sensor to the O_2/EtOH atmosphere at 593 K initiates a slight increase of XPS signal at this BE, which according to Fig. 7c corresponds to the W $4f_{5/2}$ component of the

reduced WO_x. The surface reduction of the WO_3 NWs by EtOH at high temperatures probably occurs via the interaction of the detached from the hydroxy group hydrogen atom with the WO_3 surface, forming oxygen vacancies and leaving ethoxy groups on the surface. Fig. 9b also demonstrates that the O_2/EtOH exposed surface remained similarly reduced at 493 K and completely reoxidized at 393 K due to the stopping of the hydrogen detachments.

The formation of relatively high amounts of oxygen vacancies on the surface while detecting EtOH at high temperatures, when the sensor had the most heightened sensitivity, indicated that they might contribute to the sensor response. According to the review article of Shekh et al. [43], there is still a lack of information on how oxygen vacancies influence the electrical conductivity of different metal oxides. However, studies demonstrate that they play a crucial role in the sensing mechanism of metal-oxide gas sensors [44]. To determine the effect of the surface oxygen vacancies on the electrical conductivity of the WO_3 NWs, we performed an experiment that included the formation of the surface oxygen vacancies by Ar^+ sputtering. It allowed us to create only surface oxygen vacancies and avoid the appearance of bulk defects. Before the sputtering, the sensor was cleaned and reoxidized by annealing at 593 K for about 1 h in 1 mbar of O_2, cooled to room temperature in O_2, and evacuated. The in-situ measured UHV resistance of the cleaned sensor at room temperature was approximately 240 kOhm. After that, the sensor surface was sputtered for 2 min by Ar ions at room temperature. As shown in Fig. 10a, the sputtering resulted in the partial reduction of the sensor surface. The reduction of the sensor surface dropped the sensor resistance to about 1.6 kOhm (Fig. 10b). Heating of the sputtered sensor to 593 K in UHV caused a further decrease in the sensor resistance to about 210 Ohm, which recovered only to about 1 kOhm after cooling to RT. Exposing the reduced sensor surface to 1 mbar of O_2 initiated a jump to about 1.5 kOhm. The sensor heating in the oxygen atmosphere to 593 K again caused a resistance drop to about 300 Ohm, after which it continuously increased while keeping the sensor in O_2 at 593 K. In about 1.5 h of the annealing, it increased approximately two times to 600 Ohm.

The NAP-XPS measurement performed on the surface of the sensor during the annealing in O_2 (top spectrum in Fig. 10a) showed that the concentration of the surface vacancies decreased, but still, some amount of them was present on the surface. The obtained spectrum indicated that the process of the surface reoxidation in 1 mbar of O_2 at 593 K has relatively low kinetics, probably due to the low rate of O_2 dissociation on the surface of WO_3. Finally, cooling the reoxidized sensor in O_2 to room temperature increased the sensor resistance to more than 50 kOhm. This value was five times lower than the sensor resistance before sputtering but was much higher than the resistance of the freshly sputtered sensor.

The performed experiments demonstrated that the oxygen vacancies on the surface of the WO_3 NWs strongly influence their electrical conductivity and should contribute to the sensor response in the detection of EtOH. Indeed, despite the higher amount of adsorbed EtOH at 393 K, the response at this temperature was much lower. As no surface vacancies were detected and no oxygen ionosorption is expected at this operating temperature, the sensor response is likely related to the direct adsorption of EtOH molecules working as electron donors. In contrast, the sensor response at 593 K was four times higher than at 393 K, suggesting the presence of additional sensing mechanisms contributing to it. It is the formation of relatively high concentrations of oxygen vacancies, which we detected by XPS. There might also be an effect connected with a decrease in the concentration of the ionosorbed oxygen, adsorption sites for which the adsorbed EtOH and ethoxy species might block. It is not easy to distinguish the contributions of each mechanism. However,

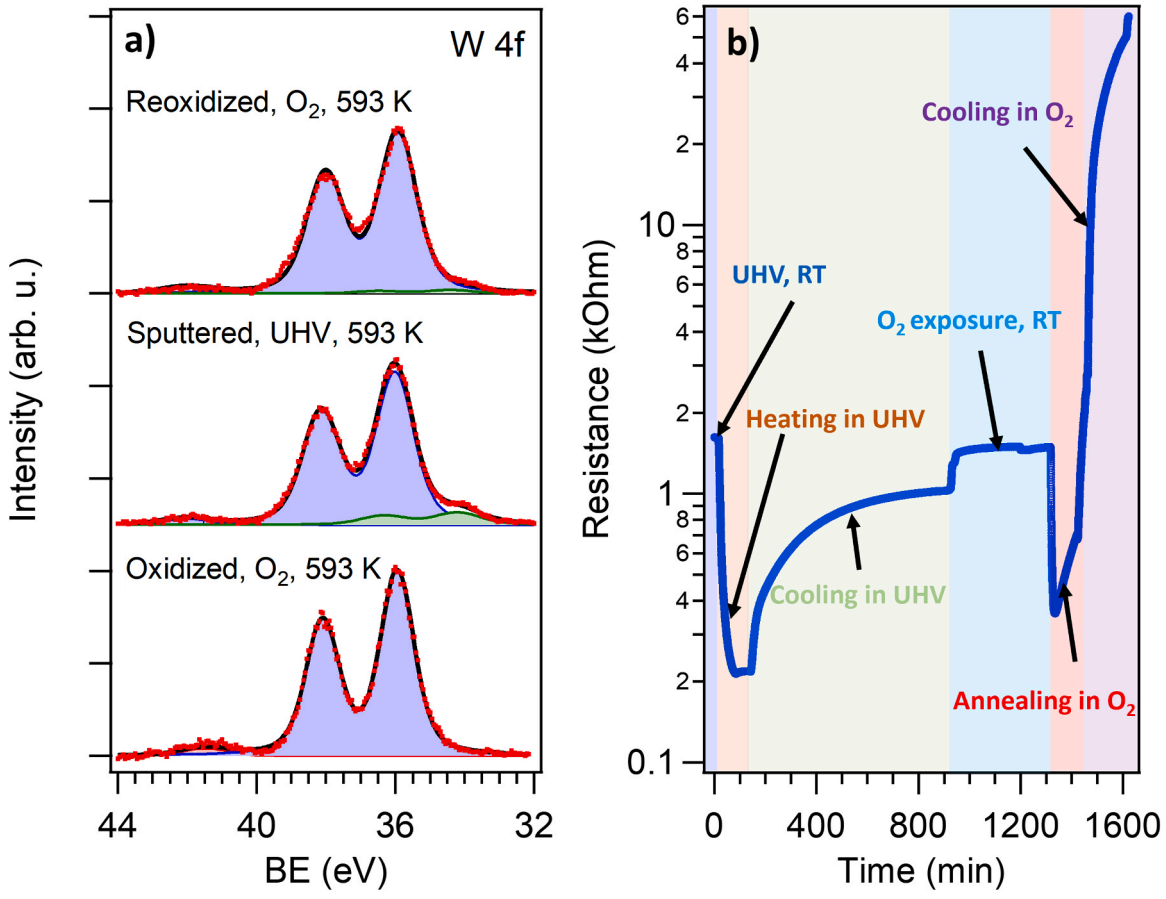

Fig. 10. (a) W 4f NAP-XPS spectra acquired from the oxidized WO_3 NWs-based sensor in O_2 at 593 K, the sputtered sensor in UHV at 593 K, and the reoxidized sensor in 1 mbar of O_2 at 593 K. (b) presents the evolution of the sputtered sensor resistance upon different treatments.

our work clearly shows that all of them should be considered when describing the EtOH detection mechanism of the WO_3 NWs-based sensor.

4. Conclusions

In this study, we have successfully performed the NAP-XPS investigation of the surface chemistry of 1D WO_3 nanostructures-based gas sensors when detecting NO_x, CO, and ethanol. The results demonstrated that long-term annealing in lower pressure of oxygen after synthesis might be insufficient to obtain a WO_3 NWs-based gas sensor suitable for the NAP-XPS study due to high carbon contamination on their surface, coming from the air exposure. We developed a methodology based on exposing the sensor to NO_x to get a clean surface that allowed the detection of tiny chemical changes while exposing it to different carbon-containing analytes. The NAP-XPS study of the CO and EtOH gas sensing mechanisms of the WO_3 NWs revealed that they combine several sensing models generally reported for the metal-oxide chemiresistors. The CO sensing does not appear to include long-term adsorption of CO molecules on the WO_3 NWs surface accompanied by electron donation. The sensor response rather arises from the quick interaction of CO with the surface oxygen atoms, which decreases the concentration of ionosorped oxygen and creates an almost undetectable amount of surface oxygen vacancies. In the case of EtOH sensing, the situation is more complicated. It is shown that from 393 K up to 593 K, the chemiresistor surface contains adsorbed ethanol molecules and ethoxy species, which could provide electrons to the surface. It is the main driving force for the macroscopic electrical response of the sensor at lower temperatures without oxygen ionosorption and surface reduction. This observation is consistent with the references [10,20], where the so-called "direct adsorption model" was proposed. Increasing the sensor operating temperature to 593 K significantly increased its response, indicating additional sensing mechanisms. Those are a strong reducing effect of EtOH on the WO_3 surface detected by XPS and the decrease in the concentration of the ionosorbed oxygen, for which the adsorbed EtOH and ethoxy species block adsorption sites.

CRediT authorship contribution statement

Lesia Piliai: Conceptualization, Data curation, Formal analysis, Investigation, Methodology, Writing – review & editing. **Thu Ngan Dinhová:** Conceptualization, Data curation, Formal analysis, Investigation, Methodology, Writing – review & editing. **Martin Janata:** Investigation, Methodology. **Dmytro Balakin:** Investigation, Methodology. **Stella Vallejos:** Investigation, Methodology, Writing – review & editing. **Jaroslav Otta:** Investigation, Methodology. **Jitka Štefková:** Investigation, Methodology. **Ladislav Fišer:** Investigation, Methodology. **Přemysl Fitl:** Data curation, Formal analysis, Investigation, Methodology, Writing – review & editing. **Michal Novotný:** Data curation, Formal analysis, Investigation, Methodology, Writing – review & editing. **Jaromir Hubálek:** Conceptualization, Data curation, Formal analysis, Investigation, Methodology, Funding acquisition, Project administration, Validation, Writing – review & editing. **Michael Vorochta:** Conceptualization, Data curation, Formal analysis, Investigation, Methodology, Funding acquisition, Project administration, Validation, Writing – original draft, Writing – review & editing. **Iva Matolinová:** Data curation, Formal analysis, Methodology, Resources, Writing – review & editing. **Martin Vrňata:** Conceptualization, Data curation, Formal analysis, Investigation, Methodology, Funding acquisition, Project administration, Validation, Writing – original draft, Writing – review & editing.

Declaration of Competing Interest

The authors declare that they have no known competing financial interests or personal relationships that could have appeared to influence the work reported in this paper.

Data availability

Data will be made available on request.

Acknowledgments

The authors acknowledge the support of the Czech Science Foundation (GAČR) - Project No. 22-14886S. CERIC-ERIC Consortium is also acknowledged for providing access to its facilities.

Appendix A. Supporting information

Supplementary data associated with this article can be found in the online version at doi:10.1016/j.snb.2023.134682.

References

[1] P.J. Shaver, Aatived tungsten oxide gas detectors, Appl. Phys. Lett. 11 (1967) 255–257, https://doi.org/10.1063/1.1755123.
[2] V. Hariharan, B. Gnanavel, R. Sathiyapriya, V. Aroulmoji, A review on tungsten oxide (WO3) and their derivatives for sensor applications, Int. J. Adv. Sci. Eng. 5 (2019) 1163–1168, https://doi.org/10.29294/ijase.5.4.2019.1163-1168.
[3] C. Dong, R. Zhao, L. Yao, Y. Ran, X. Zhang, Y. Wang, A review on WO3 based gas sensors: Morphology control and enhanced sensing properties, J. Alloy. Compd. 820 (2020), 153194, https://doi.org/10.1016/j.jallcom.2019.153194.
[4] G. Lei, C. Lou, X. Liu, J. Xie, Z. Li, W. Zheng, J. Zhang, Thin films of tungsten oxide materials for advanced gas sensors, Sens. Actuators B Chem. 341 (2021), 129996, https://doi.org/10.1016/j.snb.2021.129996.
[5] A. Yadav, P. Singh, G. Gupta, Dimension dependency of tungsten oxide for efficient gas sensing, Environ. Sci. Nano 9 (2022) 40–60, https://doi.org/10.1039/d1en00872b.
[6] M.A. Butler, R.D. Nasby, R.K. Quinn, Tungsten trioxide as an electrode for photoelectrolysis of water, Solid State Commun. 19 (1976) 1011–1014, https://doi.org/10.1016/0038-1098(76)90642-6.
[7] A. Doyan, Susilawati, L. Muliyadi, S. Hakim, H. Munandar, M. Taufik, The effect of dopant material to optical properties: energy band gap tin oxide thin film, J. Phys. Conf. Ser. 1816 (2021), https://doi.org/10.1088/1742-6596/1816/1/012114.
[8] J. Zhang, X. Liu, G. Neri, N. Pinna, Nanostructured materials for room-temperature gas sensors, Adv. Mater. 28 (2016) 795–831, https://doi.org/10.1002/adma.201503825.
[9] Y.S. Kim, S.C. Ha, K. Kim, H. Yang, S.Y. Choi, Y.T. Kim, J.T. Park, C.H. Lee, J. Choi, J. Paek, K. Lee, Room-temperature semiconductor gas sensor based on nonstoichiometric tungsten oxide nanorod film, Appl. Phys. Lett. 86 (2005) 1–3, https://doi.org/10.1063/1.1929872.
[10] A.A. Abokifa, K. Haddad, J. Fortner, C.S. Lo, P. Biswas, Sensing mechanism of ethanol and acetone at room temperature by SnO2 nano-columns synthesized by aerosol routes: theoretical calculations compared to experimental results, J. Mater. Chem. A 6 (2018) 2053–2066, https://doi.org/10.1039/C7TA09535J.
[11] Y. Wang, J. Liu, X. Cui, Y. Gao, J. Ma, Y. Sun, P. Sun, F. Liu, X. Liang, T. Zhang, G. Lu, NH3 gas sensing performance enhanced by Pt-loaded on mesoporous WO3, Sens. Actuators B Chem. 238 (2017) 473–481, https://doi.org/10.1016/j.snb.2016.07.085.
[12] S. Wei, J. Zhao, B. Hu, K. Wu, W. Du, M. Zhou, Hydrothermal synthesis and gas sensing properties of hexagonal and orthorhombic WO3 nanostructures, Ceram. Int. 43 (2017) 2579–2585, https://doi.org/10.1016/j.ceramint.2016.11.064.
[13] C.E. Brown, S.A. Mitchell, P.A. Hackett, Association reactions of nickel atoms with carbon monoxide and alkenes at room temperature: binding energy of NiC2H4, Chem. Phys. Lett. 191 (1992) 175–181, https://doi.org/10.1016/0009-2614(92)85388-Q.
[14] J. Lu, C. Xu, L. Cheng, N. Jia, J. Huang, C. Li, Acetone sensor based on WO3 nanocrystallines with oxygen defects for low concentration detection, Mater. Sci. Semicond. Process. 101 (2019) 214–222, https://doi.org/10.1016/j.mssp.2019.05.038.
[15] R. Balzer, V. Drago, W.H. Schreinerc, L.F.D. Probsta, Synthesis and structure-activity relationship of a WO3 catalyst for the total oxidation of BTX, J. Braz. Chem. Soc. 25 (2014) 2026–2031, https://doi.org/10.5935/0103-5053.20140187.
[16] H. Zheng, J.Z. Ou, M.S. Strano, R.B. Kaner, A. Mitchell, K. Kalantar-Zadeh, Nanostructured tungsten oxide - properties, synthesis, and applications, Adv. Funct. Mater. 21 (2011) 2175–2196, https://doi.org/10.1002/adfm.201002477.
[17] Q.Q. Jia, H.M. Ji, D.H. Wang, X. Bai, X.H. Sun, Z.G. Jin, Exposed facets induced enhanced acetone selective sensing property of nanostructured tungsten oxide, J. Mater. Chem. A 2 (2014) 13602–13611, https://doi.org/10.1039/c4ta01930j.
[18] H. Liu, Y. Xu, X. Zhang, F. Wei, Influence of structural orientation of tungsten oxide films on gas sensing properties, Sens. Actuators A Phys. 349 (2023), 114021, https://doi.org/10.1016/j.sna.2022.114021.
[19] S. Americo, E. Pargoletti, R. Soave, F. Cargnoni, M.I. Trioni, G.L. Chiarello, G. Cerrato, G. Cappelletti, Unveiling the acetone sensing mechanism by WO3

chemiresistors through a joint theory-experiment approach, Electrochim. Acta 371 (2021), 137611, https://doi.org/10.1016/j.electacta.2020.137611.
[20] A. Staerz, S. Somacescu, M. Epifani, T. Kida, U. Weimar, N. Barsan, WO3-based gas sensors: identifying inherent qualities and understanding the sensing mechanism, ACS Sens. 5 (2020) 1624–1633, https://doi.org/10.1021/acssensors.0c00113.
[21] L. Piliai, D. Tomeček, M. Hruška, I. Khalakhan, J. Nováková, P. Fitl, R. Yatskiv, J. Grym, M. Vorokhta, I. Matolínová, M. Vrňata, New insights towards high-temperature ethanol-sensing mechanism of zno-based chemiresistors, Sensors 20 (2020) 1–14, https://doi.org/10.3390/s20195602.
[22] A. Gurlo, R. Riedel, In situ and operando spectroscopy for assessing mechanisms of gas sensing, Angew. Chem. Int. Ed. 46 (2007) 3826–3848, https://doi.org/10.1002/anie.200602597.
[23] A. Sharma, C.S. Rout, Advances in understanding the gas sensing mechanisms byin situandoperandospectroscopy, J. Mater. Chem. A 9 (2021) 18175–18207, https://doi.org/10.1039/d1ta05054k.
[24] H.R. Kim, A. Haensch, I.D. Kim, N. Barsan, U. Weimar, J.H. Lee, The role of NiO doping in reducing the impact of humidity on the performance of SnO2-based gas sensors: synthesis strategies, and phenomenological and spectroscopic studies, Adv. Funct. Mater. 21 (2011) 4456–4463, https://doi.org/10.1002/adfm.201101154.
[25] D. Degler, B. Junker, F. Allmendinger, U. Weimar, N. Barsan, Investigations on the temperature-dependent interaction of water vapor with tin dioxide and its implications on gas sensing, ACS Sens. 5 (2020) 3207–3216, https://doi.org/10.1021/acssensors.0c01493.
[26] D. Degler, N. Barz, U. Dettinger, H. Peisert, T. Chassé, U. Weimar, N. Barsan, Extending the toolbox for gas sensor research: operando UV/vis diffuse reflectance spectroscopy on SnO2-based gas sensors, Sens. Actuators B Chem. 224 (2016) 256–259, https://doi.org/10.1016/j.snb.2015.10.040.
[27] Z. Cao, Z. Jiang, L. Cao, Y. Wang, C. Feng, C. Huang, Y. Li, Lattice expansion and oxygen vacancy of α-Fe2O3 during gas sensing, Talanta 221 (2021), 121616, https://doi.org/10.1016/j.talanta.2020.121616.
[28] A.K. Elger, C. Hess, Elucidating the mechanism of working SnO2 gas sensors using combined operando UV/Vis, Raman, and IR spectroscopy, Angew. Chem. Int. Ed. 58 (2019) 15057–15061, https://doi.org/10.1002/anie.201908871.
[29] D. Degler, S. Rank, S. Müller, H.W. Pereira De Carvalho, J.D. Grunwaldt, U. Weimar, N. Barsan, Gold-loaded tin dioxide gas sensing materials: mechanistic insights and the role of gold dispersion, ACS Sens. 1 (2016) 1322–1329, https://doi.org/10.1021/acssensors.6b00477.
[30] R.M. Palomino, R. Hamlyn, Z. Liu, D.C. Grinter, I. Waluyo, J.A. Rodriguez, S.D. Senanayake, Interfaces in Heterogeneous Catalytic Reactions: Ambient Pressure XPS as a Tool to Unravel Surface Chemistry, 2017. ⟨https://doi.org/10.1016/j.elspec.2017.04.006⟩.
[31] L. Nguyen, F.F. Tao, Y. Tang, J. Dou, X.J. Bao, Understanding catalyst surfaces during catalysis through near ambient pressure X-ray photoelectron spectroscopy, Chem. Rev. 119 (2019) 6822–6905, https://doi.org/10.1021/acs.chemrev.8b00114.
[32] M. Vorokhta, I. Khalakhan, M. Vondráček, D. Tomeček, M. Vorokhta, E. Marešová, J. Nováková, J. Vlček, P. Fitl, M. Novotný, P. Hozák, J. Lančok, M. Vrňata, I. Matolínová, V. Matolín, Investigation of gas sensing mechanism of SnO2 based chemiresistor using near ambient pressure XPS, Surf. Sci. 687 (2018) 284–290, https://doi.org/10.1016/j.susc.2018.08.003.
[33] P. Hozák, M. Vorokhta, I. Khalakhan, K. Jarkovská, J. Cibulková, P. Fitl, J. Vlček, J. Fara, D. Tomeček, M. Novotný, M. Vorokhta, J. Lančok, I. Matolínová, M. Vrňata, New insight into the gas-sensing properties of CuOx nanowires by near-ambient pressure XPS, J. Phys. Chem. C 123 (2019) 29739–29749, https://doi.org/10.1021/acs.jpcc.9b09124.
[34] D. Tomecek, M. Hruska, P. Fitl, J. Vlcek, E. Maresova, S. Havlova, L. Patrone, M. Vrnata, Phthalocyanine photoregeneration for low power consumption chemiresistors, ACS Sens. 3 (2018) 2558–2565, https://doi.org/10.1021/acssensors.8b00922.
[35] S. Vallejos, I. Gràcia, J. Bravo, E. Figueras, J. Hubálek, C. Cané, Detection of volatile organic compounds using flexible gas sensing devices based on tungsten oxide nanostructures functionalized with Au and Pt nanoparticles, Talanta 139 (2015) 27–34, https://doi.org/10.1016/j.talanta.2015.02.034.
[36] N. Minh Vuong, D. Kim, H. Kim, Porous Au-embedded WO 3 Nanowire Structure for Efficient Detection of CH4 and H2S, Sci. Rep. 5 (2015) 1–13, https://doi.org/10.1038/srep11040.
[37] C. Navío, S. Vallejos, T. Stoycheva, E. Llobet, X. Correig, R. Snyders, C. Blackman, P. Umek, X. Ke, G. Van Tendeloo, C. Bittencourt, Gold clusters on WO 3 nanoneedles grown via AACVD: XPS and TEM studies, Mater. Chem. Phys. 134 (2012) 809–813, https://doi.org/10.1016/j.matchemphys.2012.03.073.
[38] A.P. Shpak, A.M. Korduban, M.M. Medvedskij, V.O. Kandyba, XPS studies of active elements surface of gas sensors based on WO3-x nanoparticles, J. Electron Spectrosc. Relat. Phenom. 156–158 (2007) 172–175, https://doi.org/10.1016/j.elspec.2006.12.059.
[39] G. Greczynski, L. Hultman, Impact of sample storage type on adventitious carbon and native oxide growth: X-ray photoelectron spectroscopy study, Vacuum 205 (2022), 111463, https://doi.org/10.1016/j.vacuum.2022.111463.
[40] D.R. Mullins, P.M. Albrecht, Acetaldehyde adsorption and reaction on CeO2(100) thin films, J. Phys. Chem. C 117 (2013) 14692–14700, https://doi.org/10.1021/jp404752m.
[41] E. Ciftyurek, Z. Li, K. Schierbaum, Adsorbed oxygen ions and oxygen vacancies: their concentration and distribution in metal oxide chemical sensors and influencing role in sensitivity and sensing mechanisms, Sensors 23 (2023), https://doi.org/10.3390/s23010029.
[42] A. Gurlo, Interplay between O2 and SnO2: oxygen ionosorption and spectroscopic evidence for adsorbed oxygen, ChemPhysChem 7 (2006) 2041–2052, https://doi.org/10.1002/cphc.200600292.
[43] M. Al-Hashem, S. Akbar, P. Morris, Role of oxygen vacancies in nanostructured metal-oxide gas sensors: a review, Sens. Actuators B Chem. 301 (2019), 126845, https://doi.org/10.1016/j.snb.2019.126845.
[44] S. Kucharski, P. Ferrer, F. Venturini, G. Held, A.S. Walton, C. Byrne, J. A. Covington, S.K. Ayyala, A.M. Beale, C. Blackman, Direct in situ spectroscopic evidence of the crucial role played by surface oxygen vacancies in the O2-sensing mechanism of SnO2, Chem. Sci. 13 (2022) 6089–6097, https://doi.org/10.1039/d2sc01738e.

Lesia Piliai is a Ph.D. student at the Department of Surface and Plasma Science at Charles University, Czech Republic. She received her MS degree from the Department of Molecular and Medical Biophysics at Karazin Kharkiv National University, Ukraine. Her scientific work includes in-situ/operando research on gas sensors, thin film catalysts, and nano-functional materials.

Thu Ngan Dinhová is a Ph.D. student at the Department of Surface and Plasma Science at Charles University, Czech Republic. Her research includes the development and investigation of efficient nanostructured materials for the detection and elimination of volatile organic compounds from the air.

Martin Janata received his BS degree from the Faculty of Mathematics and Physics at Charles University in 2023. He is a research assistant at the Department of Surface and Plasma Science, Charles University, Czech Republic. His research interests include nanomaterials and their potential gas-sensing and biomedical applications.

Dmytro Balakin is a researcher at the University of Chemistry and Technology in Prague, Czech Republic. He received his Ph.D. from the Institute of Physics of the National Academy of Sciences of Ukraine in 2013. His current research includes the study of the catalytic properties of nanostructured materials using various spectroscopic methods.

Stella Vallejos received her Ph.D. degree in Electronic Engineering from the Universitat Rovira i Virgili, Spain. She holds a Ramón y Cajal fellowship in the IMB-CNM (CSIC). Her research focuses on gas-sensing technologies and nanomaterials for environmental and safety applications.

Jaroslav Otta is a Ph.D. student in the Department of Physics and Measurements at the University of Chemistry and Technology Prague, Czech Republic. His research activities focus on preparing and characterizing thin nanocomposite films for chemical sensors.

Jitka Štefková obtained her MSc. degree (branch Measuring Technics and Sensorics) at the Univesity of Chemistry and Technology in Prague. Her research interests are the synthesis of nanostructured oxides for chemiresistors and the measurement of sensor responses in dc- mode.

Ladislav Fišer completed his master's degree (1985) in Measurement technology in the chemical and food industry at the University of Chemistry and Technology Prague, where he also completed his Ph.D. in Measuring Technology (1999). His research now focuses on the development of gas sensors, especially chemiresistors, and the preparation of calibration mixtures for these sensors.

Přemysl Fitl is a researcher at the University of Chemistry and Technology in Prague, Czech Republic. He received his Ph.D. degree from the Czech Technical University in 2006. His research focuses on the development of highly sensitive nanostructured layers for gas sensors using different deposition techniques.

Michal Novotný is an Assistant Professor at the University of Chemistry and Technology in Prague, Czech Republic. He received his Ph.D. degree from the Czech Technical University in 2006. His research interests include thin film deposition and the characterization of properties for energy harvesting and sensor applications.

Jaromír Hubálek is an Assistant Professor at the Brno University of Technology, Czech Republic, and leads the Smart Nanodevices group at the CEITEC consortium, Brno. His research interests are in electrochemical sensors, biosensors, and gas sensors. He has extensive experience growing nanostructures using non-lithographic template methods and designing electronic systems for sensor measurements.

Michael Vorochta received his Ph.D. from Charles University in 2013. Since 2016, he has managed the Laboratory for Operando Studies in the Department of Surface and Plasma Science. His current research focuses on nanostructured films for C1 chemistry, gas sensing, and fuel cell applications.

Iva Matolínová is a Professor at the Department of Surface and Plasma Science at Charles University in the Czech Republic. She received her Ph.D. in Physics of Surfaces and Interfaces from Charles University in 1996. Her research interests include the properties of nanomaterials, especially for hydrogen technologies and gas sensors.

Martin Vrňata is a Professor at the University of Chemistry and Technology in Prague, Czech Republic. His scientific interests focus on gas sensor research, impedance analysis, and electro-transport mechanisms in semiconductors.